Forced tropical motions

Ocean response to wind stress forcing: Yoshida Jet, Stommel model, wave response
Atmospheric response to diabatic heating: Gill model
Parameterization of the atmospheric heating as a function of surface conditions: Gill-Zebiak, Lindzen-Nigam
Thermodynamics
Simple coupled model

Forced tropical motions

$$(\partial_t+\epsilon)u-yv+\partial_x\eta=\tau_x$$
$$(\partial_t+\epsilon)v+yu+\partial_y\eta=\tau_y$$
$$(\partial_t+\epsilon)\eta+\partial_x u+\partial_y v=-Q$$

Forcing includes wind stress and diabatic heating, dissipation is parameterized as Rayleigh friction and Newtonian cooling. Replace the rate of change with the combination or rate of change and dissipation, and the algebra remains as discussed previously.
The amplitude of the forcing results from the projection of the stress or diabatic heating onto vertical modes. It is therefore sensitive to the mixing parameterization. As the simplest approach the wind stress forcing applies as a body force over the mixed layer, the diabatic heating represents deep convection and is assumed to project onto the leading mode.

The Yoshida Jet:
Consider and interior ocean independent of x and forced by a constant zonal wind stress

$$(\partial_t+\epsilon)u-yv=\tau_x$$
$$(\partial_t+\epsilon)v+yu+\partial_y\eta=0$$
$$(\partial_t+\epsilon)\eta+\partial_y v=0$$

The solution is an equatorial jet, in geostrophic balance in meridional direction, and linearly accelerating in time. The meridional velocity is constant, and away from the equator merges to the Ekman transport.

$$v=-\tau_x V$$
$$u=(1-yV)\tau_x t$$
$$\eta=-\tau_x V t$$

The solution is one valid until zonally dependent arrive from the edges of the wind stress perturbation or from the boundaries of the basin.

The Yoshida Jet

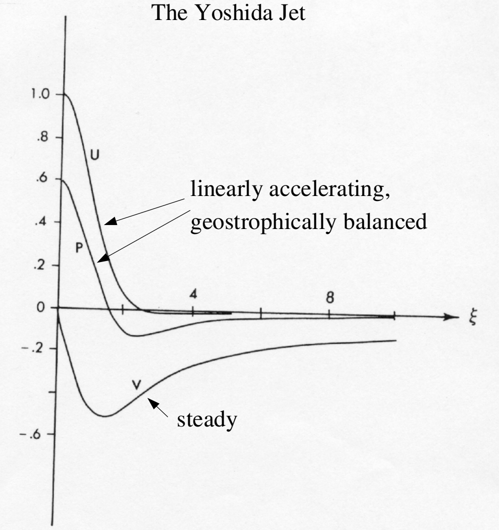

Oceanic response to wind stress forcing

Consider the spin-up problem, switch on the zonal wind stress at initial time, when flow and thermocline depth anomalies are zero (long wave limit)

$$(\partial_t+\epsilon)u-yv+\partial_x\eta=\tau_x$$
$$yu+\partial_y\eta=0$$
$$(\partial_t+\epsilon)\eta+\partial_x u+\partial_y v=0$$

The solution consists of the particular (steady) response to wind stress and a superposition of equatorial waves such that the initial condition is satisfied. The waves communicate the wind perturbation to the east (Kelvin wave) and west (Rossby waves). Upon reaching the coast the Kevlin wave spread poleward and shed westward propagating Rossby waves, while at the western coast the Rossby wave is converted to a Kelvin wave (experiencing some loss of energy due to the filtered short Rossby waves). These waves then move back into the forcing region and establish the pressure gradients that balance the wind stress.

If ϵ is small, the system will settle to a Sverdrup balance

$$-v=(\partial_x\tau_y-\partial_y\tau_x)$$
$$\partial_x u+\partial_y v=0$$

while on the equator $\partial_x\eta=\tau_x$

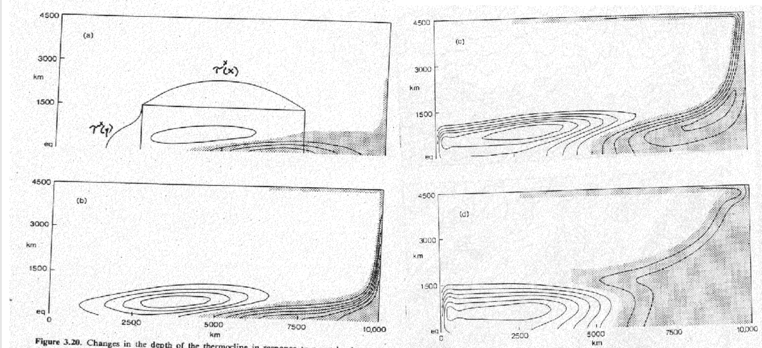

Figure 3.20. Changes in the depth of the thermocline in response to a patch of easterly winds with the zonal and latitudinal structure shown in (a). The maximum value of the windstress is 0.5 dyne/cm^2. The instantaneous pictures show conditions after (a) 1 month, (b) 3 months, (c) 13 months, and (d) 60 months. Shaded regions indicate an elevation of the thermocline. The contour interval for curves that show departures from the mean depth of the thermocline is 10 m. [From McCreary and Anderson (1984).] (*Figure continues.*)

Figure 3.20 (*Continued*)

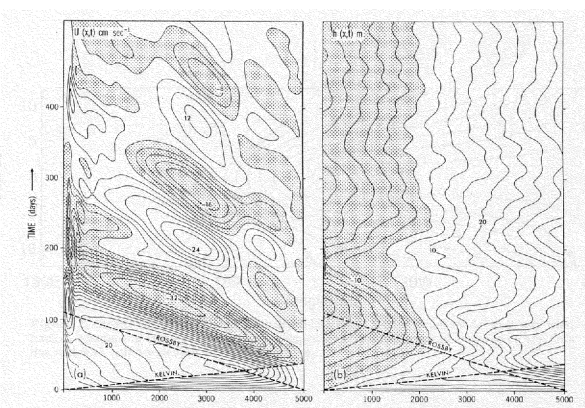

Figure 3.18. Changes in the zonal velocity component (centimeters per second) and in departures from the mean depth of the thermocline along the equator after the sudden onset of spatially uniform eastward winds. The dashed lines indicate the speeds at which Kelvin and the gravest Rossby mode propagate. The thermocline is elevated and motion is westward in shaded areas.

Philander

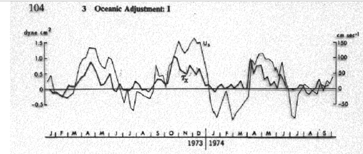

Figure 3.1. The zonal velocity component at the surface and the zonal component of the windstress, as measured in the central Indian Ocean on the equator near Gan (70°E). [From

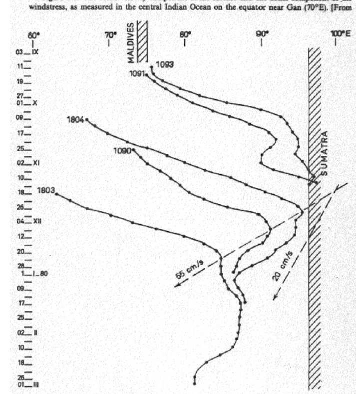

Figure 3.2. The movement of buoys that drifted with the surface currents along the equator in the Indian Ocean between 3 September 1979 and 1 March 1980. The first two buoys washed ashore on Sumatra. [From Gonella *et al.* (1981).]

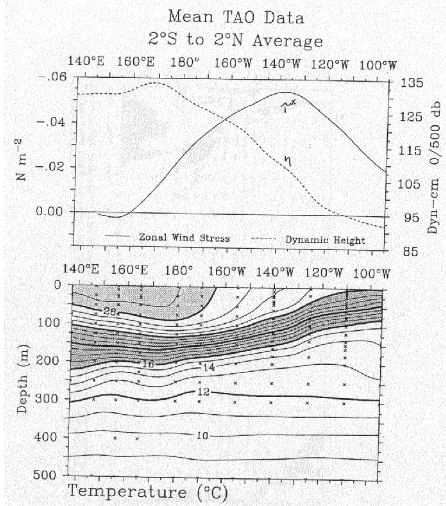

Figure 6. Zonal section of mean temperature averaged between 2°N and 2°S on the basis of available TAO time series data in 1980–1996. Also shown is the corresponding mean zonal wind stress (computed using a constant drag coefficient of 1.2×10^{-3}) and dynamic height 0–500 dbar (computed using mean temperature/salinity relationships based on work by *Levitus and Boyer* [1994] and *Levitus et al.* [1994a]). Crosses indicate depths and longitudes where temperature data were available. An average at a particular location was computed only if a minimum of 2 years of data was available.

Ekman dynamics – extension to the equator

The steady responses to a (zonal) wind stress in the inviscid limit of the 1½ layer model considered so far include no flow at the equator and no equatorial Undercurrent. This is at odds with the observed currents and temperature structure at the equator that includes a strong shear.

The vertical resolution of the model has to be increased, and the assumption of the wind stress acting as a body force over the entire active layer has to be relaxed.
A simple prototype for the effect of mixing is the Stommel model (Stommel, 1960, 'Wind drift near the equator', Deep Sea Res., 6, 298-302).

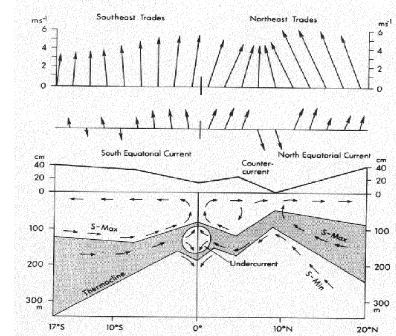

FIG. 7. Oceanographic conditions in the central equatorial Pacific between 150 and 160°W, showing winds, surface currents, dynamic height, thermal structure and meridional circulation.

Wyrtki and Kilonsky 1984

Consider a layer of constant depth, constant density, with mixing parameterized by a constant eddy exchange coefficient. The layer is forced at the surface by a wind stress, and has a free slip condition at its bottom.

$$\partial_t \vec{u} + f\vec{k} \times \vec{u} + \rho_0^{-1} \vec{\nabla} p = \partial_z A \partial_z \vec{u}$$

$$A \partial_z \vec{u} = \rho_0^{-1} \vec{\tau} \ , \ z = 0$$

$$A \partial_z \vec{u} = 0 \ , \ z = -H$$

the vertical average of these equations is $\partial_t \bar{\vec{u}} + f\vec{k} \times \bar{\vec{u}} + \rho_0 \vec{\nabla} p = (\rho_0 H)^{-1} \vec{\tau}$

while the vertical deviations from the vertical average $\vec{u}' = \vec{u} - \bar{\vec{u}}$ follow

$$\partial_t \vec{u}' + f\vec{k} \times \vec{u}' = \partial_z A \partial_z \vec{u}' - (\rho_0 H)^{-1} \vec{\tau}$$

Note that the pressure term dropped out (since $\rho = const$), and a local problem arises. (The continuity equations decoupled as well: $\vec{\nabla} \cdot \bar{\vec{u}} = 0$, $\vec{\nabla} \cdot \vec{u}' = 0$)

The solution merges the off-equatorial Ekman spiral with a down-wind on the equator and equatorial upwelling.
A two layer version of this model is implemented in the Zebiak and Cane model that will feature prominently in the discussion of ENSO.

Ekman spiral

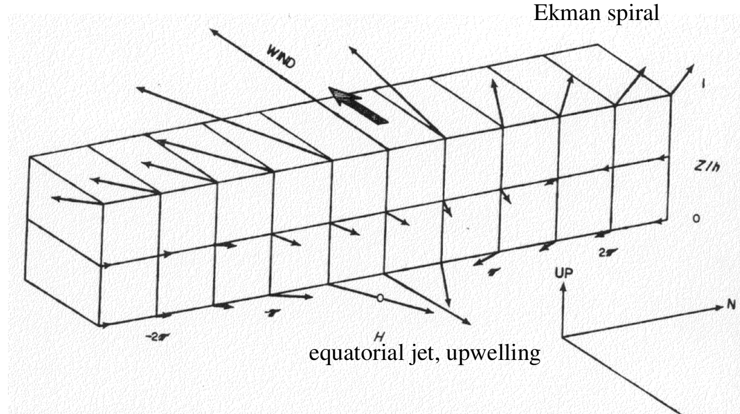

equatorial jet, upwelling

FIG. 1. Schematic three-dimensional diagram of the combined frictional and geostrophic flow field in the neighbourhood of the equator, not showing the vertical component of velocity (which can in principle be determined from continuity).

Stommel, 1959, DSR., 6, 298-302

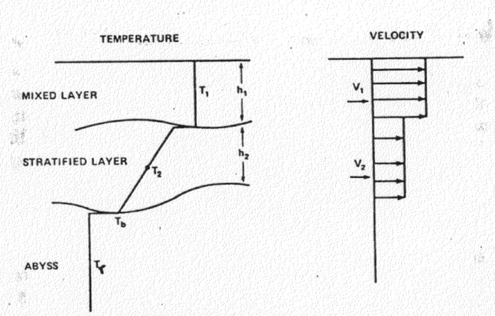

FIG. 1. Vertical structure of temperature and velocity assumed in the model equations. T_k, h_k and V_k vary with time, latitude and longitude.

Schopf and Cane, 1983, JPO, 13, 917 - 935

Forced atmospheric circulation

Interpret Q as convective latent heating that efficiently projects onto the first baroclinic mode.
Assume long wave approximation and steady state response.
Nondimensionalize equations by Rossby Radius L, L/c $c^{1/2}(2\beta)^{-1/2}, (2\beta c)^{-1/2}$

$$\epsilon u - \frac{1}{2} y v = -\partial_x p$$

$$\frac{1}{2} y u = -\partial_y p$$

$$\epsilon p + \partial_x u + \partial_y v = -Q$$

Note that in the steady limit the flow field is divergent. With the transformation $q = p + u$ and the expansion in Parabolic Cylinder functions D_i with the $r = p - u$ recursion relation

$$d_y D_n + \frac{y}{2} y D_n = n D_{n-1}$$

$$d_y D_n - \frac{y}{2} y D_n = -D_{n+1}$$

Gill, 1980, Quart. J. R. Met. Soc., 106, 447-462

and yields

$$\left.\begin{aligned} \epsilon q_0 + d_x q_0 &= -Q_0 \\ \epsilon q_{n+1} + d_x q_{n+1} - v_n &= -Q_{n+1} \ , \ n \geq 0 \end{aligned}\right\}$$

$$\epsilon r_{n-1} - d_x r_{n-1} + n v_n = -Q_{n+1} \ , \ n \geq 1$$

$$\left.\begin{aligned} q_1 &= 0 \\ r_{n-1} &= (n+1) q_{n+1} \ , \ n \geq 1 \end{aligned}\right\}$$

Example of solution with $Q = Q_0 = F(x) D_0 = F(x) e^{-(y/2)^2}$

$$\left.\begin{aligned} \epsilon q_0 + \partial_x q_0 &= -F \\ v_0 &= 0 \end{aligned}\right\} \quad \text{forced Kelvin wave}$$

$$\left.\begin{aligned} 3\epsilon q_2 - \partial_x q_2 &= -F \\ r_0 &= 2 q_2 \end{aligned}\right\} \quad \text{forced Rossby wave}$$

$$v_1 = \epsilon q_2 + \partial_x q_2$$

$$q_1 = r_1 = 0 \ , \ r_2 = v_2 = 0 \ldots$$

$$q_0(x) = -e^{-\epsilon x} \int_{-\infty}^{x} dx' e^{\epsilon x'} F(x') \qquad \text{Kelvin wave}$$

$$q_2(x) = -e^{3\epsilon x} \int_{x}^{\infty} dx' e^{-3\epsilon x'} F(x') \qquad \text{Rossby wave}$$

Kelvin wave: no response west of the forcing region, response decays with scale ϵ^{-1} to the east, meridional structure is Gaussian.

Rossby wave: no response east of the forcing region, response decays with $(3\epsilon)^{-1}$ to the west, meridional structure is D_1.

In response to heating there is poleward flow in the boundary layer due to vortex stretching.

$$q_0(x) = -e^{-\epsilon x}\int_{-\infty}^{x} dx' e^{\epsilon x'} F(x')$$ Kelvin wave

$$q_2(x) = -e^{3\epsilon x}\int_{x}^{\infty} dx' e^{-3\epsilon x'} F(x')$$ Rossby wave

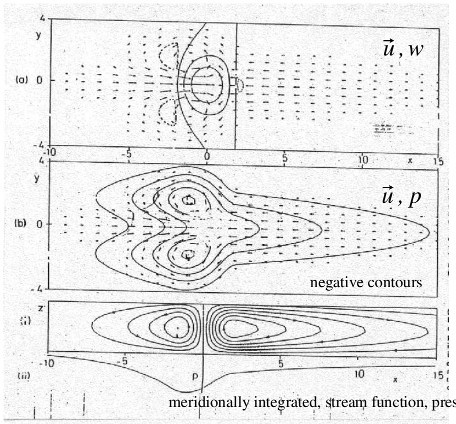

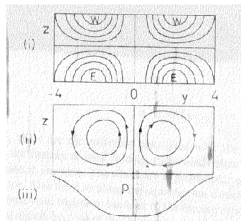

zonal average: Hadley circulation

Gill, A.E., 1980: Some simple solutiosn for heat-induced tropical circulation, Quart. J. R. Met. Soc, 106, 447-462

Response to antisymmetric forcing

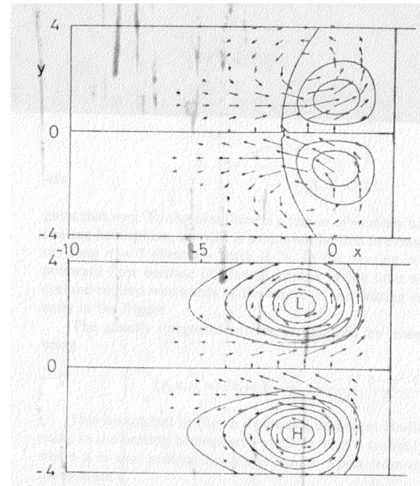

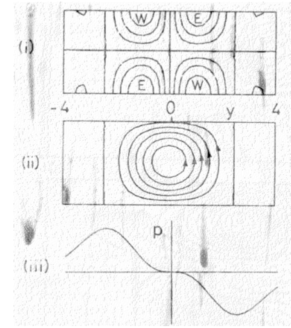

Gill 1980

Combined response

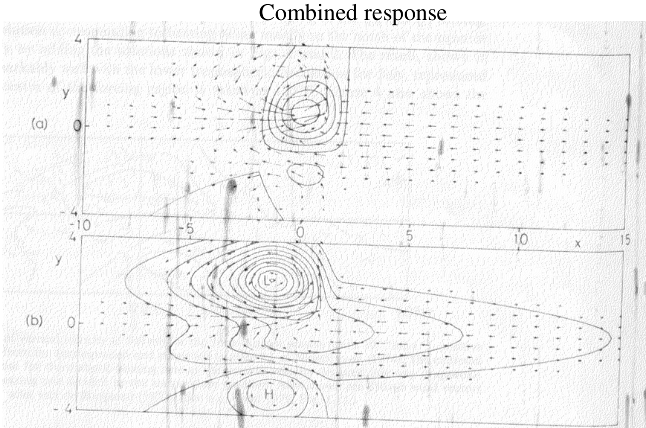

Figure 3. Solution obtained by adding the solutions shown in the two previous figures, corresponding to heating which is confined to the region $|x| < 2$ and is mainly concentrated to the north of the equator. (a) Contours of vertical velocity w (contour interval 0·3) showing the dominance of the heating north of the equator. The flow to the east of the forcing region is the same as in Fig. 1, this being provided entirely by the symmetric part of the heating. West of the forcing, the westerly inflow is concentrated between the equator and $y = 2$. An easterly flow is found south of the equator. (b) Contours of perturbation pressure p (contour interval 0·3). The pattern is dominated by a low on the western flank of the heating region and by the equatorial trough. A high is found in the southern hemisphere.

Gill 1980

How to specify Q?

Gill 1980: interpreted Q as latent heat release in deep convection.
How can the latent heat release be simulated as a function of surface conditions?

ENSO simulations of Gill and Rasmusson (1983), Nature, 306, 229-234 approximated Q as a function of OLR, and noted a relationship of OLR with migration of the region of highest sea surface temperatures.

Zebiak 1982, JAS, 39, 2017-2027 assumed Q=Q(SST), and based the formalism on local evaporation. Model resemble observations in the western and central equatorial Pacific, but fails in the eastern Pacific and South Pacific.

09/1982 12/1982

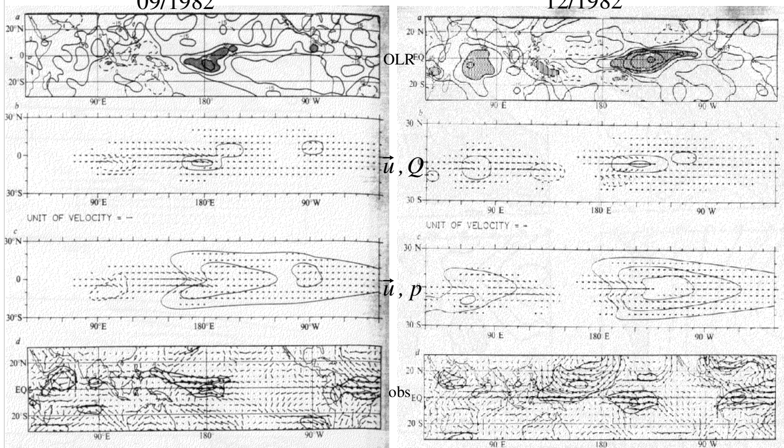

Fig. 3 *a*, Monthly mean value for September 1982 of outgoing long-wave radiation (OLR) anomaly in Wm^{-2}. Hatched regions indicate values above 30 Wm^{-2} and stippled regions values below -30 Wm^{-2}. *b*, Model response (low-level wind anomalies shown by arrows) to heat source anomalies (solid contours at 0.2 and 1.0 units), and sink anomalies (broken contour at -0.2 units) with position and strength based on *a*. *c*, As in *b*, but with surface pressure contours (interval of 0.2 units, solid contours negative, broken contour positive). *d*, Observed 850-mbar wind anomaly. Contours represent speed with 5 m s^{-1} contour interval.

Gill and Rasmusson 1983

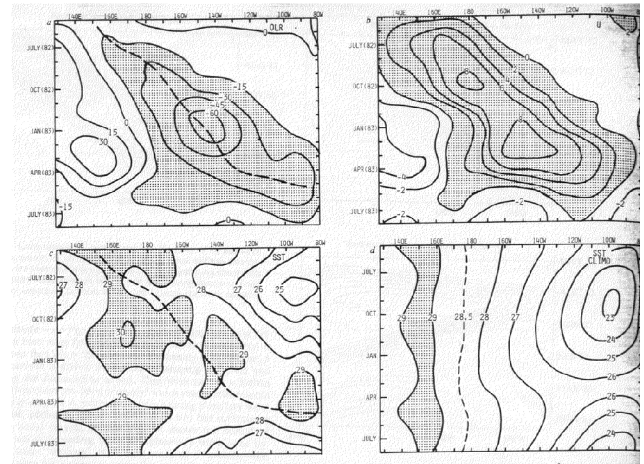

Fig. 5 Longitude–time plots along the Equator of monthly mean values of *a*, OLR anomaly during 1982–83 in Wm^{-2}. *b*, Westerly wind anomaly (5° S–5° N) during 1982–83 in ms^{-1}. *c*, SST (4° S–4° N) during 1982–83. *d*, SST climatological mean values (from ref. 33, slightly smoothed). The dashed line in *a*, *c* follows the peak OLR anomaly.

Gill and Rasmusson 1983

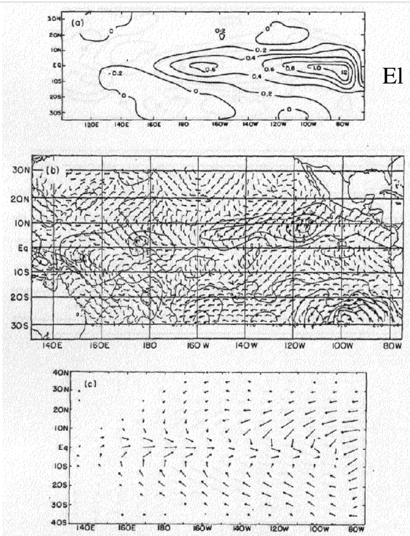

El Nino composite SST

observed composite wind

model wind

FIG. 6a. Model heating, based on the composite SST anomalies for the period centered around June, during the coastal warming.
FIG. 6b. Composite wind anomalies for the same time period as in 6a.
FIG. 6c. Model results for the heating in 6a.

Zebiak 1982, Fig. 6

But latent heat release (precipitation) is not only a function of SST but also of the moisture transport in the boundary layer.
Zebiak 1986, Mon. Wea. Rev., 14, 1263-1271

$$Q = Q_{evap}(\bar{T}, T, RH) + Q_{conv}(\bar{\vec{u}}, \vec{u}, \bar{q})$$
$$= \Gamma T' - \beta_z \vec{\nabla} \cdot \vec{u}$$

β_z is nonzero only if total wind field is convergent.

Note that the low level convergence depends on Q and affects Q and leads to an interative solution.

Further refinements such as full moisture budget have been explored (consider the moisture convergence, not just the mass convergence).

Zebiak 1986, Fig. 5

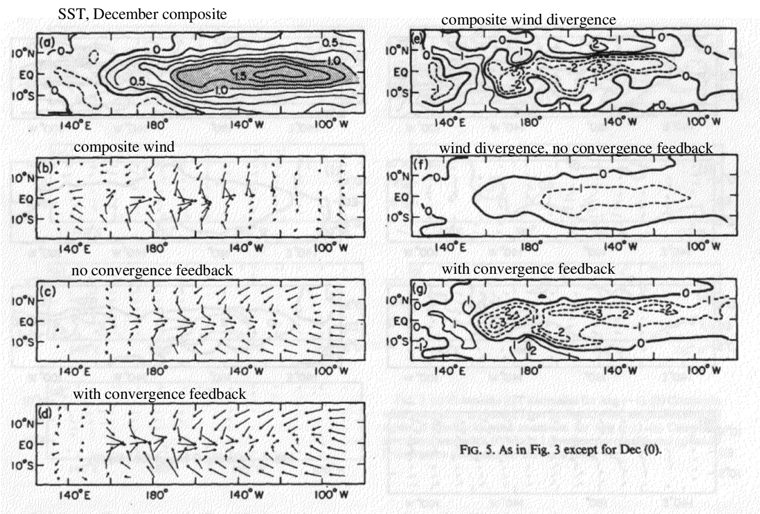

Zebiak 1986

Problems with the Gill-Zebiak model

assumes that the latent heat release in the troposphere affects flow in the boundary layer.
implies very large, local latent heat releases (and gains as a function of SST)
upper level vorticity budget is nonlinear, yet the model is linear
the phase speed of the first baroclinic mode is fast, so that a strong damping is needed to constrain the spatial extent of the atmospheric response.

Model type	Model source	Mechanical damping ϵ_D^{-1} (days)	Venting or thermal damping ϵ_T^{-1}	Wave speed m s^{-1}	Typical forcing ($W\ m^{-2}$)
Convective (full troposphere)	Gill–Zebiak	**1–2**	**1–2 days**	60	**75**
	observations	≈10	≈15 days	≈40	15–20 (evaporative)
Boundary layer	Lindzen–Nigam	≈1–2	**30 min**	≈16*	5–10 (virtual sensible)
	Reduced gravity (section 2b)	≈1–2	8 h	≈18	5–10 (virtual sensible)
	Observations	≈1–2	≈3–12 h	≈18	5–10 (virtual sensible)

Battisit et al. 1999

Lindzen and Nigam, 1987, JAS, 44, 2418-2436

considers boundary layer only
SST anomalies produce sensible and latent heat fluxes and affect the virtual temperature, and therefore pressure in the boundary layer
the temperature anomaly in the boundary layer is

$$T_a'(x,y,z)=T_v'(x,y)(1-z\gamma/H_b)$$

where H_b is the boundary layer height (700 mb height surface).

The momentum equation in the boundary layer is (the true and tried)

$$\epsilon_D\vec{u}+f\vec{k}\times\vec{u}+\vec{\nabla}\phi=0$$

Pressure is affected by temperature changes and by the fluctuating top of the boundary layer $\phi=g(1+\alpha H_b/\bar{T}_s)h+\Gamma T_v'$

which depends on the balance of the mass convergence in the boundary layer and entrainment, acting on a convective adjustment time

$$-H\vec{\nabla}\cdot\vec{u}=\epsilon_t h$$

$$\epsilon_D\vec{u}+f\vec{k}\times\vec{u}+\vec{\nabla}\phi=0$$

$$\epsilon_D\phi+c_{\ln}^2\vec{\nabla}\cdot\vec{u}=-\epsilon_D\Gamma_{\ln}T_V'$$

$$c_{\ln}^2=gh\frac{\epsilon_D}{\epsilon_T}$$

Thus, the equations of the Lindzen and Nigam model are very similar to the Gill model, but the physical interpretation and parameters are very different.

TABLE 1. Counterparts between Gill's (1980) model and the present model.

Gill (1980)	Present model
Artificial lid at tropopause	Trade inversion, Z_T
Thermal relaxation time	Cumulonimbus setup time
Artificial tropospheric friction	Surface drag
Artificial internal mode	Relatively mixed layer below Z_T
Forcing nominally due to cumulus heating	Forcing calculably due to SST distribution

Lindzen Nigam 1987

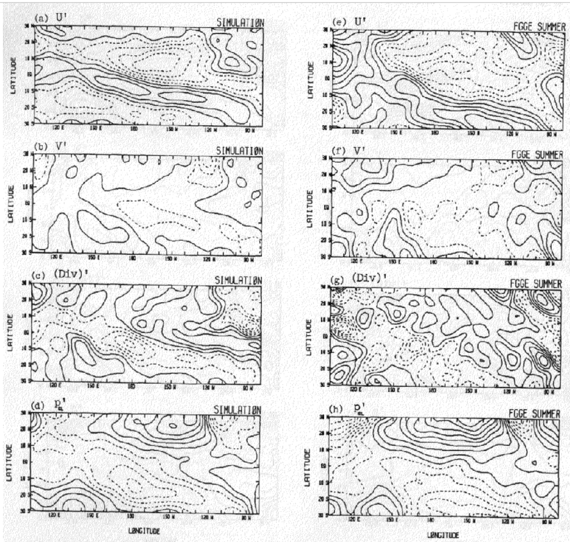

FIG. 5. The low-level summertime flow over the Pacific obtained from the linear model in which the boundary layer height is allowed to adjust to the horizontal convergence; $\epsilon = (2.5 \text{ days})^{-1}$, $\tau_c = 30$ min, $H_0 = 3000$ m. The model solutions are shown in the left panel whereas the corresponding fields from the ECMWF analysis are shown in the right panel. The contour interval is as follows: U' and $V' = 1 \text{ m s}^{-1}$, div $= 4 \times 10^{-7} \text{ s}^{-1}$, and $p'_{SL} = 1$ mb; negative values are contoured using dashed lines, and the first solid contour is the zero contour.

Lindzen and Nigam 1987

Reduced gravity model: Battisti, Sarachik, Hirst, , 12, 2956-2964

This model is similar to Lkindzen and Nigam, but the virtual temperature perturbations are well mixed in the boundary layer.
The boundary layer is capped by a constant inversion.
The free atmosphere acts to reduce gravity and to absorb mass and heat without significant flow above the boundary layer (reduced gravity).
Damping time of the boundary layer depends on its mass convergence: If convergence is diagnosed, the boundary layer height is damped rapidly (8 hrs, convection), else a slower entrainment rate of 1-2 days is assumed.

$$\epsilon_D \vec{u} + f\,\vec{k} \times \vec{u} + \vec{\nabla}\phi = 0$$

$$\epsilon_D \phi + g' H (1-\beta') \vec{\nabla} \cdot \vec{u} = -\epsilon_D \Gamma T'$$

$$\beta' = \begin{cases} 1 - \dfrac{\epsilon_d}{\epsilon_m} & \textit{if convergent} \\ 0 & \textit{else} \end{cases}$$

Form of model is again similar to Gill's model.

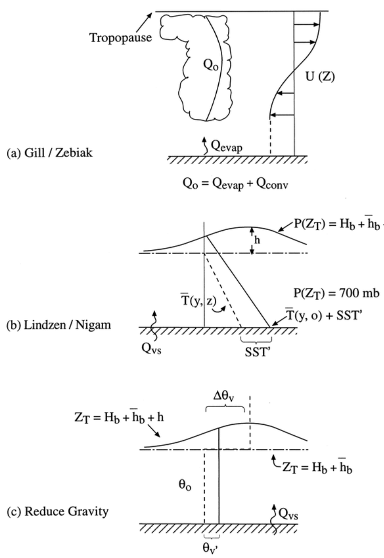

Battisti, Sarachik, Hirst, J. Clim., 12, 2956-2964, 1999

Thermodynamics of equatorial SST

To couple the ocean and atmosphere models, we need to consider SST. In the spirit of the reduced (simple) models discussed so far, consider the temperature balance of a surface mixed-layer of depth H_1 and vertically constant temperature T

$$\partial_t T + \vec{u} \cdot \vec{\nabla} T = H_1^{-1} \left[(\rho_0 c_p)^{-1} Q_{AS} - w (T - T_{subsurf}) \right]$$

The ocean model provides $\vec{u}$ and the thermocline depth h. The latter can be empirically determined.

The air-sea heat flux Q_{AS} is expressed in terms of surface temperature T and equilibrium temperature T_A

$$Q_{AS}(T) = -\alpha (T - T_A)$$

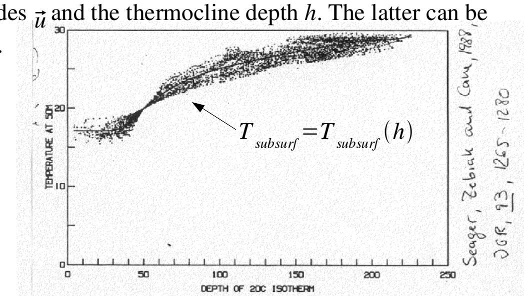

rature at 50-m depth as a function of depth of the 20°C isotherm with best fit curve derived by cubic spline method. Data are from *Levitus* [1982].

Thermocline depth and temperature at base of the mixed layer are linked in the eastern equatorial Pacific.

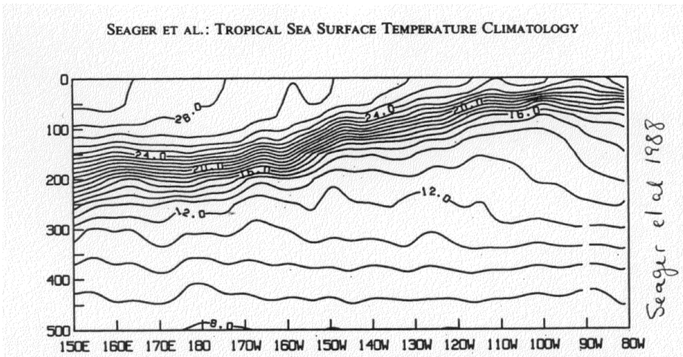

Fig. 1. Equatorial cross section of temperature for May, June, and July [after *Levitus*, 1982].

The prototype coupled model

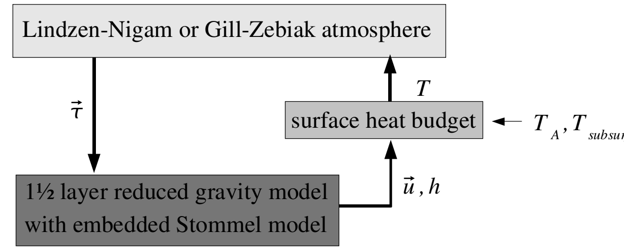

Note that the atmosphere is in steady state with the surface conditions. The ocean provides the memory and slow evolution due to thermal inertia of the mixed layer, and more importantly due to Rossby and Kelvin wave dynamics.

This model forms the basis for discussions of the coupled dynamics in the tropics